Journal of
Marine Science and Engineering

MDPI

Article

Analysis of Underwater Acoustic Propagation under the Influence of Mesoscale Ocean Vortices

Sartaj Khan [1,2,†], Yang Song [1,2,*,†], Jian Huang [1,2] and Shengchun Piao [1,2]

[1] College of Underwater Acoustic Engineering, Harbin Engineering University, Harbin 150001, China; sartaj@hrbeu.edu.cn (S.K.); a370699479@gmail.com (J.H.); shengchunpiao@hrbeu.edu.cn (S.P.)
[2] Acoustic Science Technology Laboratory, Harbin Engineering University, Harbin 150001, China
* Correspondence: song_yang@hrbeu.edu.cn; Tel.: +86-158-4650-8908
† Sartaj Khan and Yang Song contributed equally to this work.

Abstract: Mesoscale ocean vortices are common phenomenon and fairly distributed over the global oceans. In this study, mesoscale vortex in the South China Sea is identified by processing of AIPOcean data. The characteristic parameters of the identified vortex are extracted by using Okubo-Weiss (OW) method. The empirical sound velocity formula and interpolation method are used to obtain the spatial characteristics of temperature and sound velocity of the mesoscale vortex. After this, a theoretical model based on the Gaussian method is established to fit and simulate the vortex parameters. Using this model, the influence of mesoscale vortex strength, cold and warm vortex, vortex center position and sound source frequency on sound propagation are analyzed in COMSOL software. Finally, the actual parameters of the identified vortex are compared with the ideal Gaussian vortex model. It is found that different types of mesoscale vortices have different effects on the underwater sound propagation characteristics. Cold vortices, for example, cause the sound energy convergence zone to move toward the sound source, reducing the convergence zone's span, whereas warm vortices cause the sound energy convergence zone to move away from the sound source, increasing the convergence zone's span. Furthermore, the stronger the mesoscale vortices, the greater the impact on the sound field. Our COMSOL-based results are consistent with previous research, indicating that this model could be useful for studying underwater acoustic propagation in vortices.

Keywords: mesoscale vortex; acoustic propagation; AIPOcean; OW method; COMSOL software

check for updates

Citation: Khan, S.; Song, Y.; Huang, J.; Piao, S. Analysis of Underwater Acoustic Propagation under the Influence of Mesoscale Ocean Vortices. *J. Mar. Sci. Eng.* **2021**, *9*, 799. https://doi.org/10.3390/jmse9080799

Academic Editor: Grigory Ivanovich Dolgikh

Received: 28 June 2021
Accepted: 21 July 2021
Published: 24 July 2021

1. Introduction

More than 90% of the surface kinetic energy in the ocean lies in the entire ocean circulation [1], which can be seen as cyclones, anticyclones and typhoons in the ocean. The physical properties of mesoscale vortices are similar to those of cyclones and anticyclones in the atmosphere [2,3]. Mesoscale ocean vortices (named eddies) are common and fairly distributed over the global oceans. They usually existing for 10 to 100 days and have medium spatial scales in the horizontal direction ranging from 50 to 500 km [4–6]. These kinds of vortices are widely distributed in the South China Sea. Earlier, Li et al. [7] reported an anticyclonic ring detached from Kuroshio in the South China Sea. Using observation data, Wu et al. [8] analyzed sound speed field in the same region of Ref. [7] by using 2D parabolic equation (PE) algorithm. So, it is of great importance to study the ocean vortices as they largely influence the vertical structure of water column in the sea. In this way, acoustic propagation in the vortex region will be changed significantly [9]. Previous studies have determined that the loss of acoustic signal strength of sonar can be up to about 40 db in the presence of vortices [10]. The study of mesoscale vortex, therefore, has important application value for underwater acoustic equipment, underwater weapons, submarine warfare and anti-submarine warfare. Due to the importance of underwater acoustic propagation to the sonar detection and submarine navigation, it is significant for the oceanographers and acousticians to understand the mechanisms of vortex and its influence on underwater acoustic propagation.

Vortex recognition is the first step in the study of vortices in seawater. Since the 1970s, oceanographers and acousticians have studied and developed many methods for the identification of vortices. In the field of vortex recognition algorithms based on physical parameters, one of the most widely used is based on the properties of Okubo-Weiss (OW) parameter q (Okubo 1970 [11]; Weiss 1991 [12]). This parameter is used to determine the spatial structure of the vortex and to identify regions with different mixing properties [13]. The OW method is the earliest proposed and most widely used method for vortex identification [14,15], because it has a simple principle and a small amount of calculation. Chaigneau [16] used the altitude data obtained from high-resolution satellite measurements in the past 15 years to identify and compare the vortices in the waters of Peru using both the OW method and the WA method [17]. Their results showed that the average radius of the sea vortex is 80 km, and it gradually increases to the north, and the average vortex life is about 1 month. In this area, the warm vortex tends to move to the northwest, and the cold vortex tends to move to the southwest. Doglioli et al. [18] proposed a wavelet analysis method, based on the high-resolution numerical model of the seas surrounding South Africa, focusing on the study of anticyclones and cyclones in the Kepler Basin, which are believed to be actively involved in the Indian Ocean Atlantic Ocean exchange, including vortices. The calculation of the vortex trajectory and the time evolution of the vortex characteristics provide objective tools for the identification and tracking of the 3D vortex. Francesco et al. [19] developed a new method of identifying vortices based on the geometric shape of the velocity vector. The vortex is automatically identified through the spatial distribution of the velocity vector near the center of the vortex, which is a good algorithm for high-frequency radar surface velocity data for the Gulf of Southern California.

In the past, much work has been done to investigate the physical characteristics of mesoscale ocean vortices and their influence on acoustic propagation. Vastano and Owens [20] used numerical simulation technique based on the geometric acoustic model to study the effect of cold vortices on the sound propagation law of the deep-sea sound channel when the sound source was located at the center of the vortex. They used ray tracking method to describe the effect of vortex on transmission loss. A coherent ray technique was used by Weinberg and Zabalgogeazcoa [21] to investigate the effect of cold vortices on sound propagation when the sound source and receiver positions are both outside the vortex, and the results are expressed in a time series. These previous studies of acoustic transmission were based on the direct oceanographic measurements of vortex. Baer [22] used the PE method to study the propagation characteristics of sound waves in the ocean vortex field. It was found that in a vortex field, using a 100 Hz non-directional sound source, the received acoustic signal energy within the grazing angle increases by 5 to 50%. When the vortex moves along the line connecting the sound source and the receiver, the difference in the position of the vortex relative to the sound source can cause a 20 db decrease in the propagation loss. Li et al. [5] used an underwater acoustic model-MMPE to examine the acoustic propagation under the influence of different types, intensities and positions of eddies, and different frequencies and depths of sources. In recent years, Chen et al. [6] used UMPE model to analyze the acoustic propagation characteristics under the influence of cold-core vortex. For this, they selected the cold vortices based on the summer hydrological environment in the Kuroshio extension sea region. Chen et al. [23] examined the influence mechanism of eddies on acoustic propagation from the perspective of surface waveguide by Argo floats data and typical 2D ray algorithm. A fully 3D PE model was used by Heaney [24] to discover the horizontal refraction due to mesoscale eddy at low frequency acoustics in the South Indian Ocean.

This study provides an objective tool for the identification and tracking of 3D vortices. The principle and process of mesoscale vortex recognition by OW method is introduced, and a cold vortex is identified at position 15–18° N, 115–117° E in the South China Sea (Section 2). In a disparate departure from previous research, this study applies the OW method to extract and identify vortices using real time data from the AIPOcean 1.0 numerical product. A theoretical model of sound field calculation under the influence of vortex is then developed in COMSOL software [25] based on the finite element method (Section 2). Utilizing this model, the influence of mesoscale ocean vortex on sound propagation using low frequency is analyzed and discussed (Section 3). Finally, main findings and future work are summarized in Section 4.

2. Data and Methods

2.1. AIPOcean Region and Argo Data

China joined the international Argo program in 2002 and deployed 100–150 Argo buoys between 2002 and 2005 in the South China Sea, the East China Sea and the Yellow China Sea to build a regional observation network in the Pacific Northwest along the coast of China. After that, 20–30 buoys have been deployed every year to maintain the normal operation of the local observation network. At present, China has become an important member of the Argo project, providing important assistance for ocean observation in the Northwest Pacific [26]. The ocean reanalysis data set of the joined area Asia-Indian-Pacific Ocean (hereafter AIPOcean; [27]) used in this paper is the numerical product of China's Argo project, and its range is 30°–180° E, 28° S–44° N as shown in the Figure 1, the spatial resolution is about 1/4° × 1/4°. This data set contains the average 3D temperature, salinity and flow field from 1 January 1993 to 31 December 2006, as well as the 2D sea surface height. The original data is interpolated on the standard vertical plane on the isodensity coordinates.

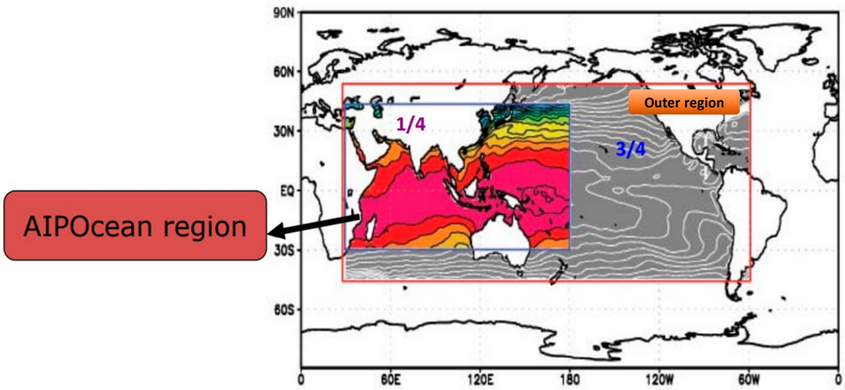

Figure 1. The geographical location of the AIPOcean region and the peripheral area used in the establishment of the grid model.

2.2. Vortex Identification and Extraction Based on OW Method

2.2.1. Vortex Identification Based on OW Method

The zonal velocity and meridional velocity data were provided by Argo buoys. These two datasets can be combined with the OW method to identify mesoscale vortices. According to the definition of OW function [11,12,28]:

$$\mathrm{w} = \frac{\partial v}{\partial x} - \frac{\partial u}{\partial y} \tag{1}$$

$$S_n = \frac{\partial u}{\partial x} - \frac{\partial v}{\partial y} \tag{2}$$

$$S_s = \frac{\partial v}{\partial x} + \frac{\partial u}{\partial y} \tag{3}$$

where S_n, S_s, and w are the normal and the shear components and vorticity of the relative vortex. (u, v) indicates the horizontal velocity, with positive values representing the east (x) and northward (y) directions. We can define the parameter q (OW parameter) as:

$$\text{q} = S_s^2 + S_n^2 - w^2 \quad (4)$$

Then a suitable q_0 is given as a threshold to determine the position of the vortex center of the mesoscale vortex. Here, $\text{q}_0 \leq -0.2\sigma_\text{q}$, which is commonly used in the research, is selected as the threshold to judge the position of the vortex center of the mesoscale vortex, where σ_q is the standard deviation of the q value.

After determining the position of the vortex center of the mesoscale vortex, it is necessary to combine the velocity field and the sea surface height field to calculate the change trend of the velocity and sea surface height in different directions. Select the location of the maximum value of the velocity in different directions within a reasonable radius as the mesoscale. The edge estimation position of the vortex, the average value of the distance between the edge position in each direction and the identified vortex center position as the radius, and finally the average gradient of the region is calculated as the intensity of the mesoscale vortex. The data related to zonal flow velocity, meridional flow velocity, temperature, salinity, etc. are obtained from AIPOcean 1.0 product. The flow chart of the OW algorithm is shown in Figure 2. As shown in the figure, the entire identification process can be divided into the following steps:

(1) Extraction of Argo buoy data: As the data of the Argo buoy are available in Network Common Data Form (NetCDF) format, it is necessary to use the ncread function in the Matlab [29] to extract the zonal flow velocity, meridional flow velocity, temperature and salinity required for identification.
(2) Delineate the scope of calculation: The extracted zonal flow velocity and meridional flow velocity exist in the form of 3D variables of latitude, longitude and height. The surface velocity at a depth of 100 m is selected and a matrix is formed in the range of $10° \times 10°$ for calculation.
(3) Calculate the value and threshold of the q parameter: After obtaining the matrix of the zonal flow velocity u and the meridional flow velocity v, the gradient function can be used to calculate the derivatives of u and v in the x and y directions, and then Equations (1)–(4) can be used to calculate the value of q. The standard deviation function is used to calculate the threshold q_0.
(4) Determine the position of the center of the mesoscale vortex: After obtaining the value of q and q_0, the position of the vortex center can be obtained by comparing the two values. After obtaining the position of the vortex center, the maximum value of the flow velocity in different directions can be selected as the edge estimation value using the flow velocity field in the Argo numerical product, and the average value of the distance from the vortex center can be used as the radius estimation value of the mesoscale vortex.

To illustrate the steps of this procedure, we will apply it to processing a selected ocean mesoscale vortex (Table 1). According to the temperature and salinity and flow velocity profiles of the Argo buoy, appropriate processing has been performed to obtain the spatial distribution characteristics of the mesoscale vortex such as temperature and sound velocity.

Table 1. Mesoscale vortex information extracted by the OW method.

Vortex Center Position	Type	Volex Radius	Maximum Flow Rate
16.74° N, 115.72° E	Cold vortex	27.055 km	15.6 cm/s

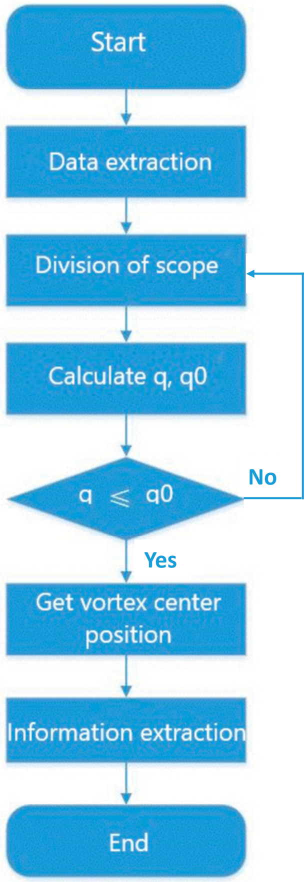

Figure 2. Flow chart of the OW algorithm.

2.2.2. Extraction of Mesoscale Vortex Spatial Characteristics

After completing the identification process of the mesoscale vortex, we start to extract the spatial characteristic information such as the temperature and sound velocity of the mesoscale vortex. The speed of sound in seawater varies from about 1500 to 1580 m/s. By extracting the temperature and salinity data in the mesoscale vortex region, the temperature and salinity distribution at a depth of 0–1000 m is obtained. Usually, the speed of sound is obtained by a special sound speed measuring tool. However, since there is no sound speed data, an empirical formula for sound speed is used here (Mackenzie, 1981 [30]):

$$\begin{aligned} C = {} & 1448.96 + 4.591T - 5.304 \times 10^{-2}T^2 + 2.374 \times 10^{-4}T^3 + 1.340(S - 35) + 1.630 \times 10^{-2}D \\ & +1.675 \times 10^{-7}D^2 - 1.025 \times 10^{-2}T(S - 35) - 7.139 \times 10^{-13}TD^3 \end{aligned} \quad (5)$$

where C = sound speed (m/s), T = temperature (°C), S = salinity (parts per thousand) and D = depth (m). Ranges of validity of this formula cover:

$$0 \leq T \leq 30, 30 \leq S \leq 40, 0 \leq D \leq 8000 \quad (6)$$

The temperature, salinity and depth data, extracted from the Argo profiles, are entered into the sound velocity empirical Formula (5) for calculation, and the distribution of the vortex sound velocity can be obtained. Figure 3a shows the distribution of isovelocity lines map at 500 m depth obtained from the Argo profiles. As can be seen from the figure, outward spreading trend in the sound velocity is observed on the right side of the vortex. The sound velocity changes are more gradual at the outer side and more intense near the center of the vortex. The isovelocity line distribution of the entire vortex can be approximated as an irregular elliptical shape, and we can further process the vortex on this basis to facilitate subsequent simulation processes. As shown in the figure, at the same depth, the sound velocity distribution of the mesoscale vortex is approximately elliptical, with a major axis radius of about 70 km.

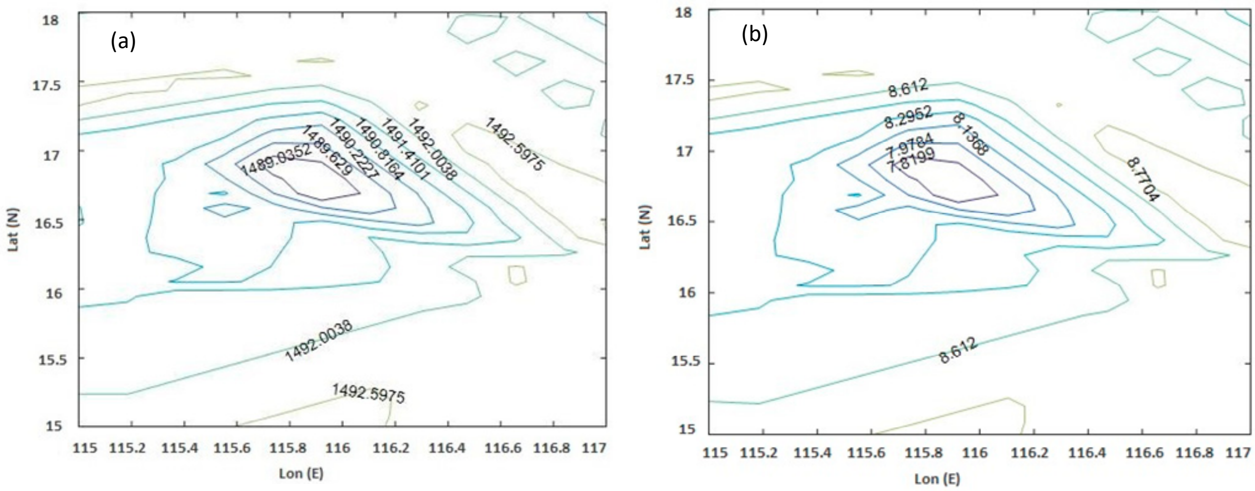

Figure 3. (**a**) Isovelocity (m/s) and (**b**) Isotemperature (°C), contour lines map at 500 m depth.

The temperature distribution of the mesoscale vortex at a depth of 500 m is shown in Figure 3b. It can be seen from the figure that the vortex center is the region with a minimum temperature. By comparing the temperature distribution and the sound velocity distribution, it is observed that the temperature distribution and the sound velocity distribution trends tend to be consistent. This is because of the three factors *T*, *S* and *D* that affect the speed of sound, the temperature T has the greatest effect on the speed of sound. The temperature distribution can be approximated to describe the sound velocity distribution characteristics of mesoscale vortices.

The temperature and sound velocity distribution of the mesoscale vortex obtained from the vertical profiles at depth range from 250 to 600 m from Argo data is given in Figure 4. The temperature and speed of sound are consistent with the temperature and speed of sound at the edge of the vortex. The vortex parameters obtained from Argo buoy data are shown in Table 2.

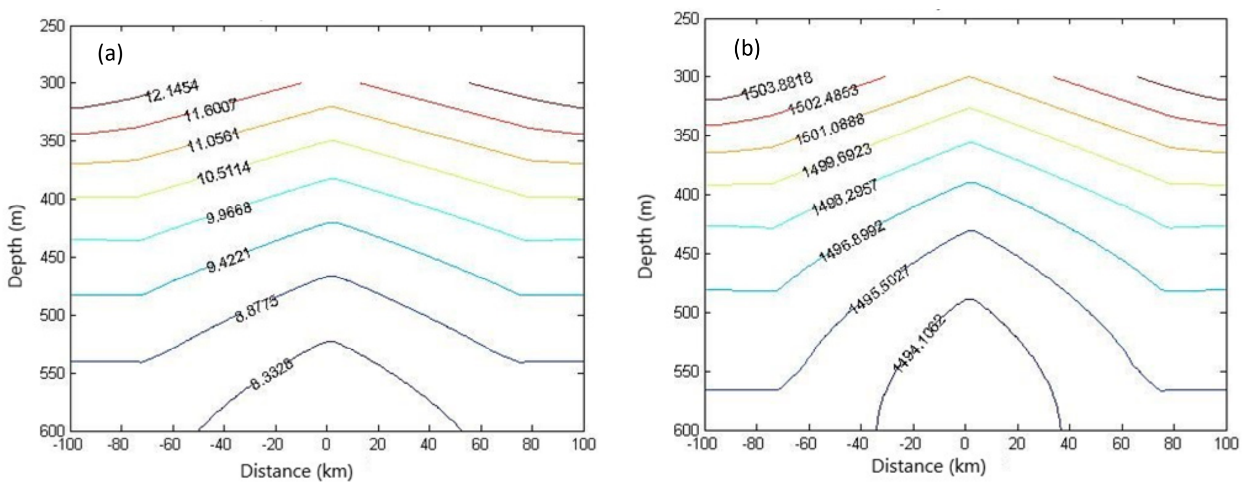

Figure 4. (**a**) Isotemperature (°C) and (**b**) Isovelocity (m/s), contour lines map at a depth range of 250 to 600 m.

Table 2. Vortex parameters based on Argo Buoy data.

Depth z/m	Vortex Center Position		Vortex Size at Different Depths		Vortex Center Temp (T_0/°C)	Vortex Edge Temp (T_1/°C)	Temperature Difference between Edge and Center (°C)
	x_0/m	y_0/m	x_m/km	y_m/km			
300	270	−135	96.9	71.7	11.45	12.69	1.24
400	170	−185	76.0	59.6	9.68	10.48	0.80
500	160	−147	73.6	52.4	8.51	9.25	0.74
600	453	−204	63.0	49.5	7.77	8.46	0.69

A linear interpolation method is applied to obtain the temperature of the mesoscale vortex region. The required mesoscale vortex parameters are: vortex center position (x_0, y_0) relative to the coordinates given in Table 1, vortex size (x_m, y_m), vortex center temperature (T_0/°C) etc. and the environment temperature $T(x,y,z)$ is:

$$T(x, y, z) = T_0(z) + [T_1(z) - T_0(z)]r(x, y) \tag{7}$$

And,

$$\frac{[x - x_0(z)]^2}{{x_m}^2(z)} + \frac{[y - y_0(z)]^2}{{y_m}^2(z)} = r^2(x, y) \tag{8}$$

where $0 \leq r(x,y) \leq 1$, $z_{min} \leq z \leq z_{max}$, $r(x,y) < 1$ present the effective area of the vortex, and $r(x,y) > 1$ is the area in which the temperature and sound velocity are consistent with the temperature and sound velocity of the vortex edge.

T_1 and z represent depth of vortex and temperature at vortex edge, respectively. x_0 and y_0 represent the position of vortex center, they are determined by maximum or minimum temperature horizontal position of vortex. Using interpolation methods (Equations (6) and (7)) and empirical sound velocity formula (Equation (5)), the simulated sound velocity distribution and temperature distribution of the mesoscale vortex at different depths are shown in Figure 5a–f. By comparing Figures 4 and 5, it can be seen that even under different depth planes, the sound velocity distribution and temperature distribution still tend to be consistent, which validates Equation (6).

2.3. Modeling of Mesoscale Ocean Vortex

2.3.1. Fitting of Vortex Parameters Based on Gaussian Method

After obtaining the spatial characteristic parameters of the mesoscale vortex in the previous section, in this study we take the actual parameters at a depth of 400 m in Table 2, as an example, to fit the ideal Gaussian vortex model [31], and establish a mesoscale vortex model based on this. Table 3 shows the main parameters of mesoscale vortices selected from Table 2.

Table 3. Mesoscale vortex parameters.

Vortex Depth	Short Half Axis	Long Half Axis	Temperature Difference between Vortex Edge and Vortex Center	Sound Velocity Difference between Vortex Edge and Vortex Center
400 m	29.8 km	38 km	0.8 °C	3.6 m/s

Taking an ideal Gaussian vortex as an example, the effect of the existence of a vortex on a 2D plane in the vertical direction on the speed of sound is [5,20,31]:

$$\delta_c(x, y, z) = DC * \exp[-(\frac{r - r_e}{DR})^2 - (\frac{z - z_e}{DZ})^2] \tag{9}$$

In the formula, DC represents the intensity of the vortex, and the value of DC is the maximum difference in sound velocity from the center of the vortex to the edge of the vortex.

The value of DC is negative for the cold vortex, and DC is positive for the warm vortex. DR is the horizontal radius and DZ is the vertical radius of the vortex. The horizontal and vertical positions of the vortex center are represented by r_e and z_e, respectively. By putting the main parameters of the mesoscale vortex in Table 3 into the ideal Gaussian vortex model Equation (8), we will obtain the Gaussian vortex model parameters that conform to the actual sound velocity distribution. The sound velocity distribution obtained by this method is shown in Figure 6.

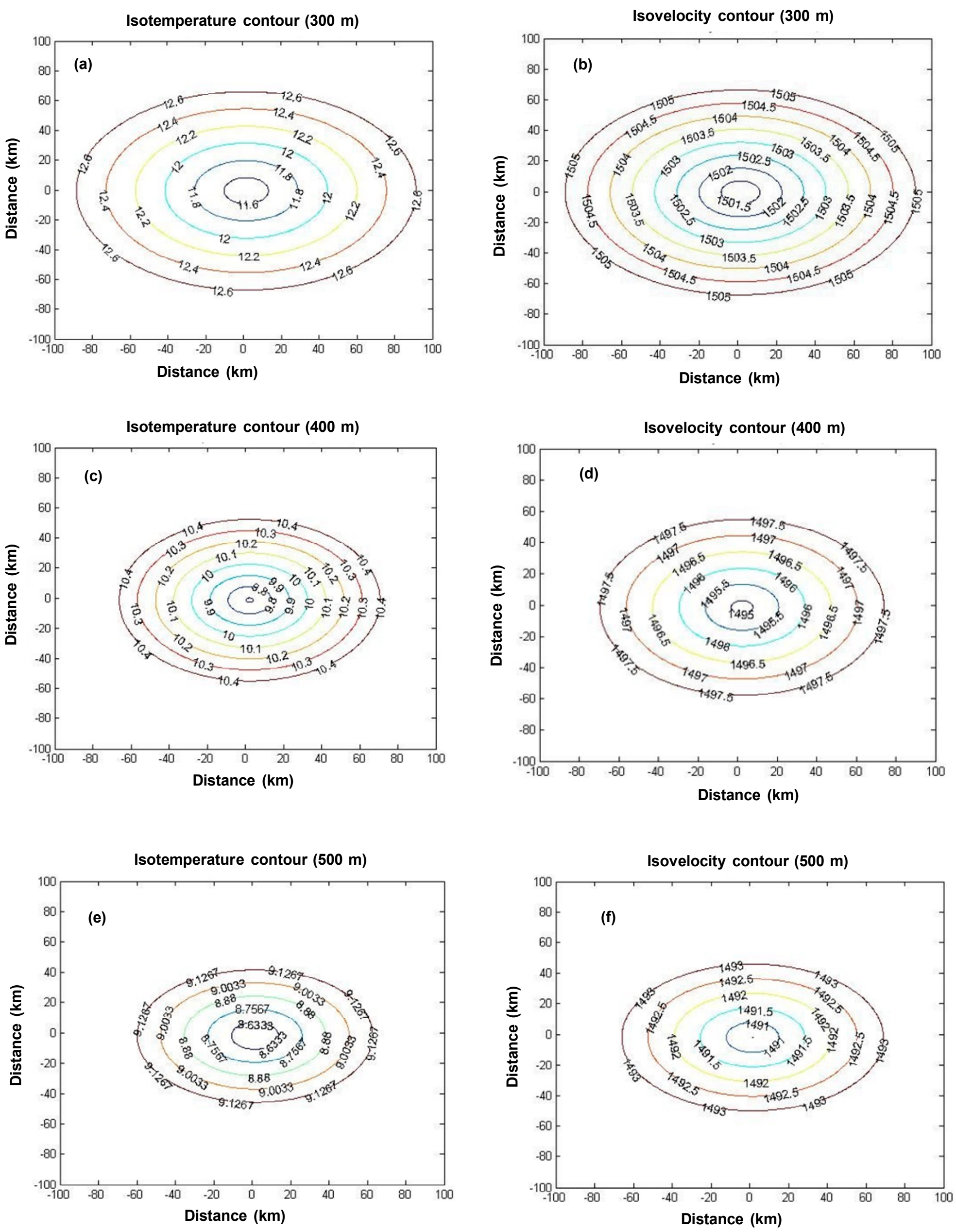

Figure 5. Interpolation plots of temperature (°C) distribution in the horizontal direction at different depths and the corresponding interpolation distribution plots of sound velocity (m/s): (**a**,**c**,**e**) Isotemperature contour is 300, 400 and 500 m, (**b**,**d**,**f**) Isovelocity contour is 300, 400 and 500 m.

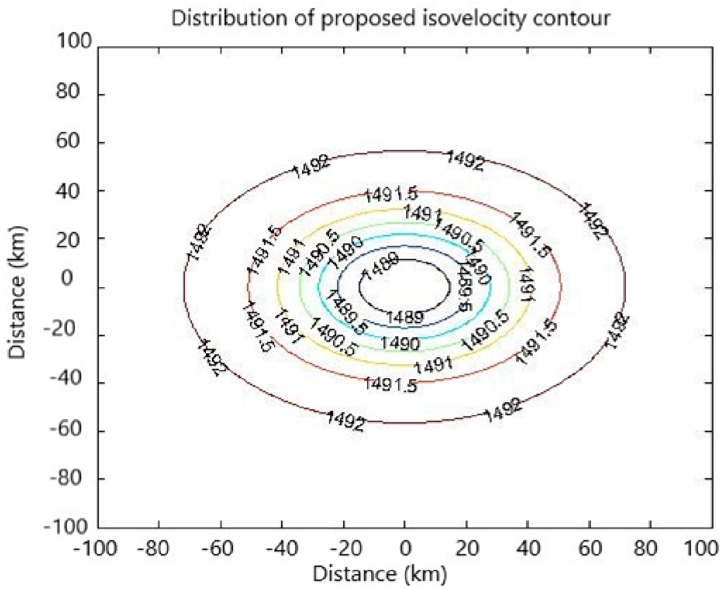

Figure 6. Sound velocity (m/s) distribution image obtained by Gaussian fitting method.

For comparison, we superimpose the sound velocity distribution field obtained from the in-situ data (Figure 3a) on the sound velocity distribution field obtained by the fitting data (Figure 6). By qualitatively comparing Figures 3a and 6, it is found that the distribution of the sound velocity gradient tends to be roughly the same. The distribution trends show the mesoscale vortex in the ideal state, but it also reflects the characteristics of the actual data, such as the rising trend of sound velocity from large to small, and the slower the change of sound velocity is closer to the edge. It can be considered that the fitting data better reflects the actual data, and the vortex model can be used for simulation.

2.3.2. Sound Field Modeling Based on COMSOL Finite Element Method

According to the law of sound propagation, at the deep sound speed channel, when the sound waves emitted by a sound source placed near the sea surface, they will reverse at a certain depth and return to the vicinity of the surface again and form a convergence zone. This reversal depth is generally between 4000 and 5000 m, and the position of the first convergence zone is about 40 km from the source. Based on these factors such as the inversion depth, the distance of the convergence zone, and the size of the vortex, Gaussian vortex model [30] is adopted to describe the ocean mesoscale vortex (Figure 7a,b).

The upper layer of the model is a seawater medium, and the lower seafloor is set as a liquid seafloor, which directly simulates the presence of mesoscale vortices in the seawater medium in the form of sound velocity distribution. COMSOL will select the physical field before building the model. Since this model uses a liquid seabed and only considers pressure acoustics, the physical field is set to pressure acoustics, frequency domain and steady state is selected for the research direction.

Due to the existence of mesoscale vortices, the sound velocity of seawater in this model is:

$$c(x,y,z) = c_0(z) + \delta_c(x,y,z) \tag{10}$$

In the formula, $c_0(z)$ is the standard model of SOFAR sound velocity profile proposed by Munk [32]:

$$c_0(z) = 1500\{1 + \varepsilon[e^{-\eta} - (1-\eta)]\} \tag{11}$$

where $\eta = 2 * (z - z_0)/B$, z is depth, z_0 is the minimum depth of the sound velocity model and taken as 1000 m, B is the waveguide width and its value is 1000 m, ε is the magnitude of deviation from the minimum value and its value is 0.0057, proposed by Munk [32]. According to the Formula (10), the vertical distribution of the deep-sea sound channel, when there is no vortex, is shown in Figure 7b. In Equation (8), $\delta_c(x,y,z)$ indicates the influence of the existence of mesoscale vortices on the distribution of sound velocity in seawater.

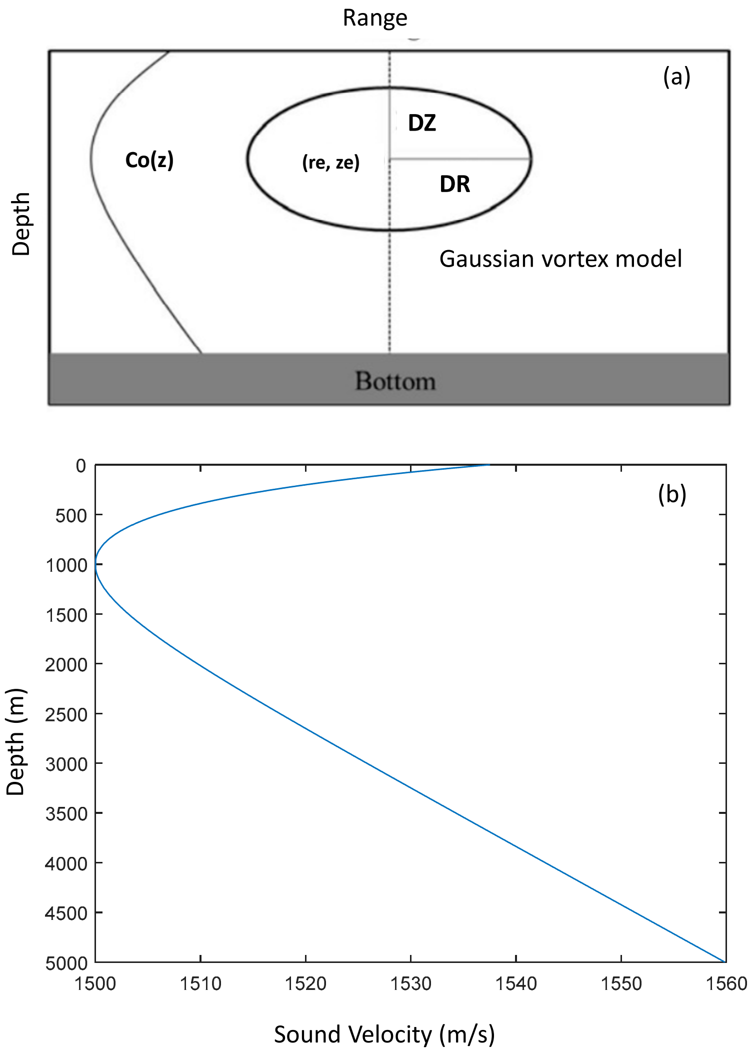

Figure 7. (**a**) Schematic diagram of the 2D model of Gaussian Ocean Vortex, (**b**) Vertical distribution of deep-sea sound channel.

3. Results and Discussion

3.1. The Influence of Mesoscale Vortices on Sound Propagation

3.1.1. The Influence of Vortex Intensity on Sound Propagation

Consider the impact of mesoscale vortex intensity on sound propagation first. Based on the mesoscale vortex model established in Section 2, we choose 5 vortices with varying vortex strengths for simulation experiments. We take a non-directional point sound source with a frequency of 20 Hz, a depth of 200 m, and DC values of −20 m/s, −10 m/s, 0, 10 m/s, and 20 m/s, respectively. A negative DC value indicates a cold vortex, a positive DC value indicates a warm vortex, and a DC value of 0 indicates there is no vortex. For this, the vortex's center is set to be the same distance as the sound source, i.e., Rx = 20,000 m, while all other conditions remain constant. Figures 8–10 show the simulation results of the sound pressure level distribution for cold vortices, without vortices and warm vortices, respectively.

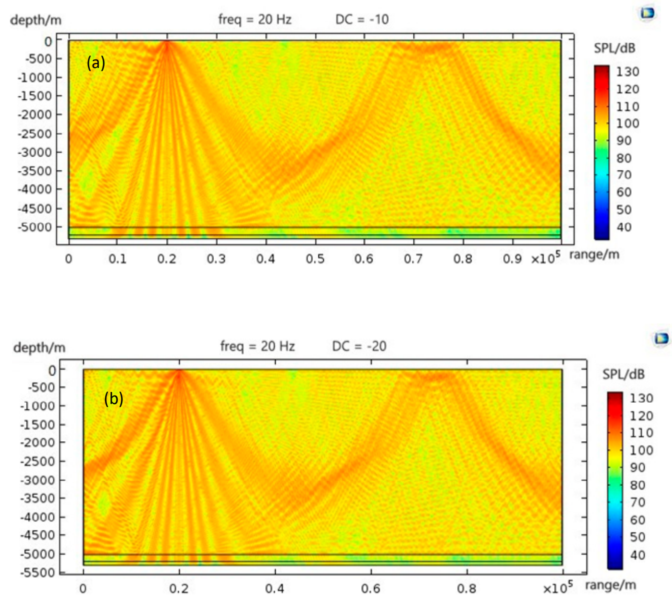

Figure 8. The distribution of sound pressure level under different intensities of cold vortex, (**a**) DC = −10 m/s and (**b**) DC = −20 m/s.

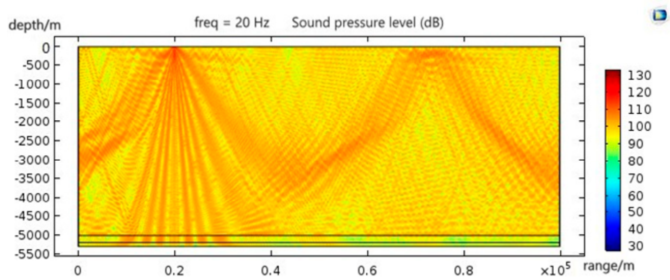

Figure 9. Sound pressure level (dB) distribution when there is no vortex (DC = 0).

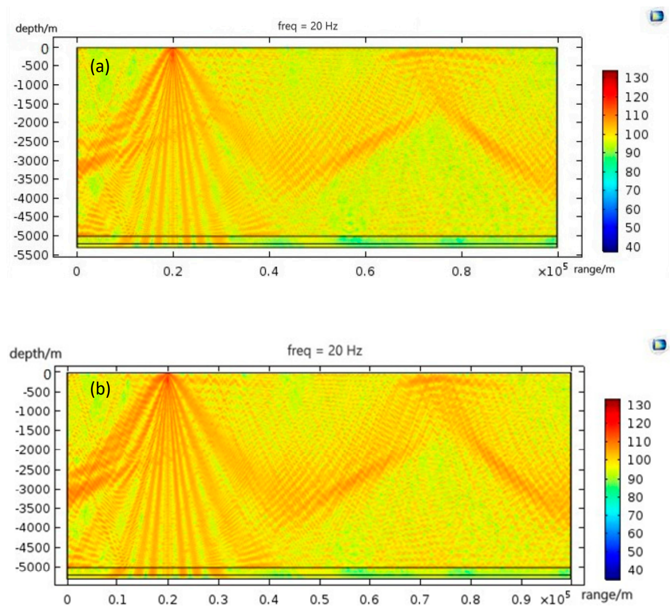

Figure 10. Distribution of sound pressure levels (dB) under different intensities of warm vortices, (**a**) DC = 20 m/s and (**b**) DC = 10 m/s.

The transmitting sound wave bends in the direction of the lower sound velocity region due to the uneven environment of sound velocity distribution in seawater. As a result, in the deep-sea channel, the sound rays are inverted and propagated upward, forming a 'sound energy convergence zone' near the sea surface in the positive sound velocity gradient region below the channel axis. The deep-sea channel's first convergence zone is frequently found at 45–50 km. Figure 10 shows that a significant amount of sound energy is concentrated about 50 km away from the sound source, which is significantly higher than in other regions.

In Figures 8–10, the convergence zone first appears at 45 km from the sound source when DC = −10 m/s (Figure 8a); when DC = 0 (Figure 9), the convergence zone appears at 50 km from the sound source; when DC = 10 m/s (Figure 10b), the convergence zone appears at about 55 km away from the sound source; and when DC = 20 m/s (Figure 10a), the convergence zone appears at about 60 km away from the sound source. We can conclude from this that when there is a cold vortex, the converging zone moves in the direction of the sound source; when there is a warm vortex, the converging zone moves away from the sound source. Furthermore, the convergence effect of sound rays is weakened when there is a warm vortex. The width of the entire convergence area is enlarged, and in an environment where there is a cold vortex, the sound rays converge more densely and appear darker in the sound pressure level distribution image. Figure 11 depicts the vertical distribution of sound velocity in seawater with different intensities of mesoscale vortices. Figure 12 depicts the deep-sea channel distribution of the vertical section drawn through the vortex's center. It can be seen from figures that the effect of the vortex on the speed of sound mainly exists in the region close to the sea surface, which is about 0–1000 m deep.

The sound velocity distribution of the vertical section of the model without and with mesoscale vortex is located (see Figure 11), are obtained by applying our COMSOL-based model. From these figures, we can observe that the sound velocity is significantly changed after the mesoscale vortex appears: the isovelocity line bends upwards with the vortex core in the center, and forms an elliptical low-sound velocity zone which is more dominant in the central region. The distribution of iso-sound velocity lines is consistent with the actual sound velocity distribution obtained by interpolation method in Section 2.3.1, which can prove that this method can better simulate the sound velocity distribution of the sound field in the presence of mesoscale vortices. It is demonstrated that when DC = 20 m/s (Figures 11a and 12), the warm vortex will cause a depth of 0–1000 m, i.e., the sound velocity gradient of the upper part of the channel axis will become smaller near the sea surface, and the rapid change in the part close to the channel axis will be positive. When DC = −20 m/s (Figure 11c and Figure 12), the cold vortex even causes a sound velocity gradient to appear at a depth of about 500 m that is lower than the sound velocity of the channel axis, reducing the positive sound velocity gradient from 1000 m to 500 m. The mesoscale vortices are thought to change the properties of the sound field and influence the distribution of the sound velocity gradient, thereby influencing sound propagation. Some of the stronger vortices even altered the nature of the sound velocity gradient, such as a cold vortex with DC = −20 m/s (Figure 11c and Figure 12), which moves the positive gradient up and expands the negative gradient.

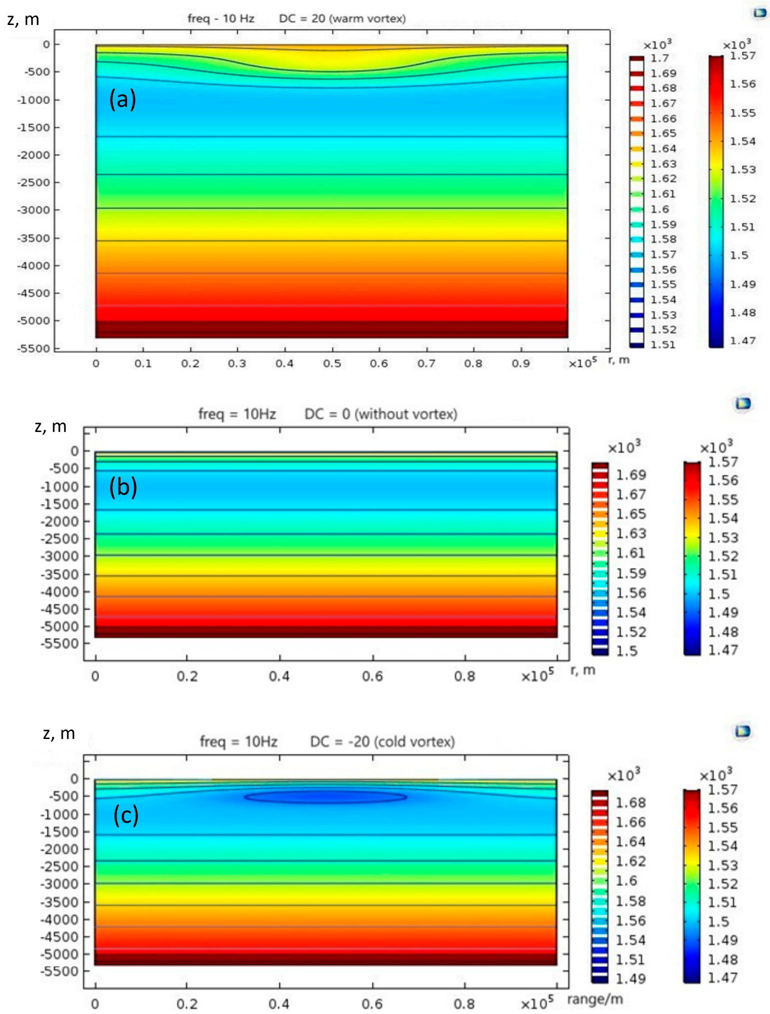

Figure 11. The vertical plane of sound velocity (m/s) distribution when vortices with different DC values exist (**a**) DC = −20 m/s, (**b**) DC = 0, and (**c**) DC = 20 m/s.

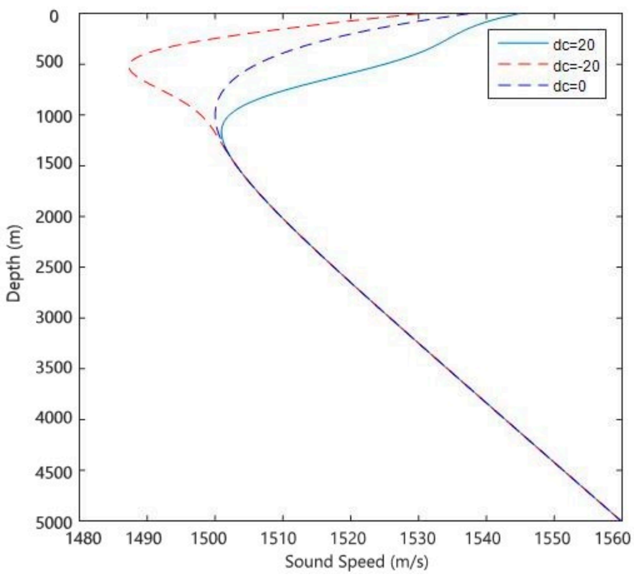

Figure 12. Distribution of the deep-sea sound channel in the vertical section of the vortex center.

3.1.2. The Influence of Vortex Position on Sound Propagation

Given that the vortex affects sound propagation by changing the sound velocity distribution in the seawater, the vortex's influence on the sound velocity distribution at different positions in the sound field must be different as well. This section discusses the effect of the vortex on sound propagation at various positions. The sound pressure level distribution when the sound source is located at the center of the vortex is shown in Figure 13. The sound velocity distributions of the cold vortex at different positions in the sound field are presented in Figure 14a,b. We can see from Figure 14 that when the sound source is set at the center of the vortex, the convergence zone moves away from the sound source. Furthermore, the depth of the convergence zone has decreased by about 100 m from its original depth.

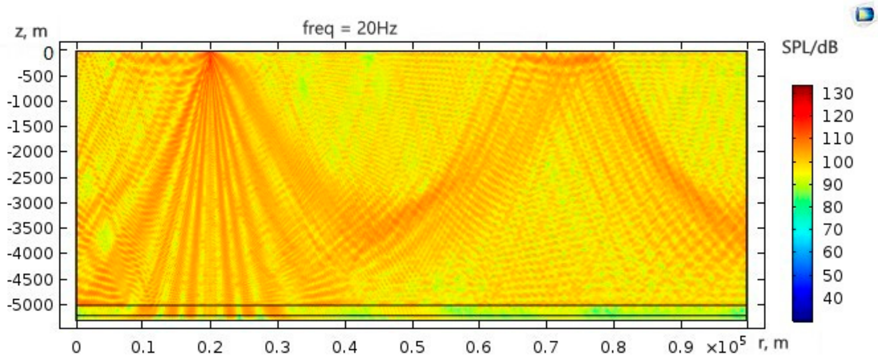

Figure 13. Sound pressure level distribution when the sound source is located at the center of the vortex (DC = −20 m/s).

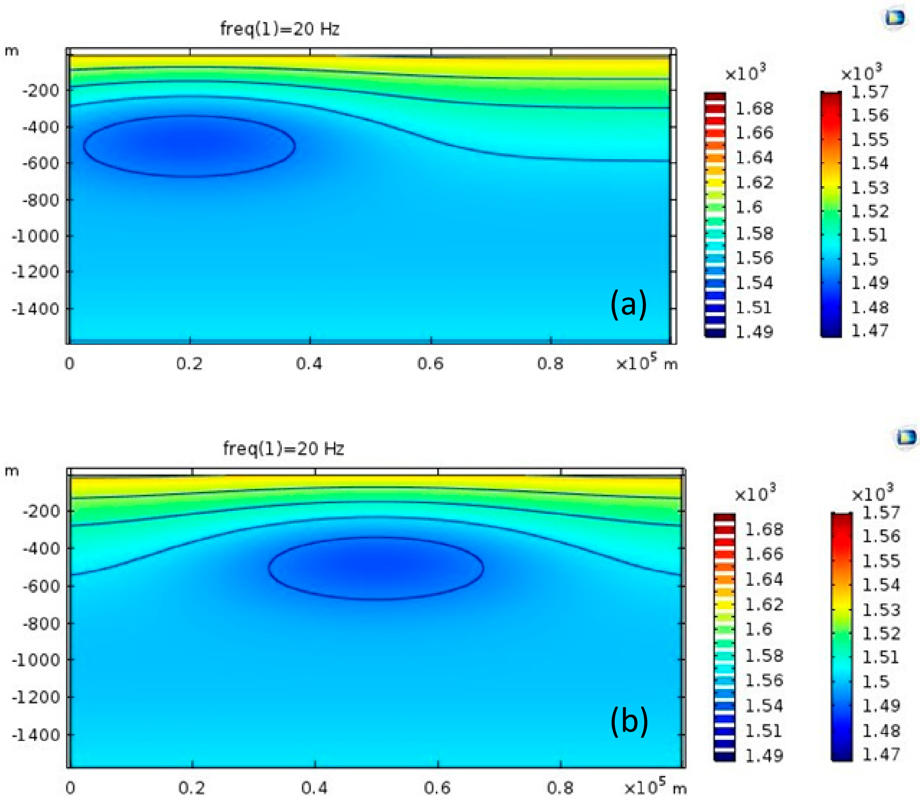

Figure 14. The sound velocity distribution of the cold vortex at different positions in the sound field, (**a**) Rx = 20,000 m, DC = −20 m/s, (**b**) Rx = 50,000 m, DC = −20 m/s.

Now, using the vortex center as the origin, we draw the change in sound velocity gradient at various distances from the vortex center. Variation in sound velocity gradient at different distances are shown in Figure 15a–e. The sound velocity gradient changes from a negative gradient in the upper half to a positive gradient in the lower half, and then gradually changes to a uniform negative gradient, which is the distribution of the sound velocity gradient in the absence of a vortex. As the sound waves are affected by the sound velocity gradient as they propagate, the sound waves bend to the lower sound velocity location, and the height of the convergence zone decreases.

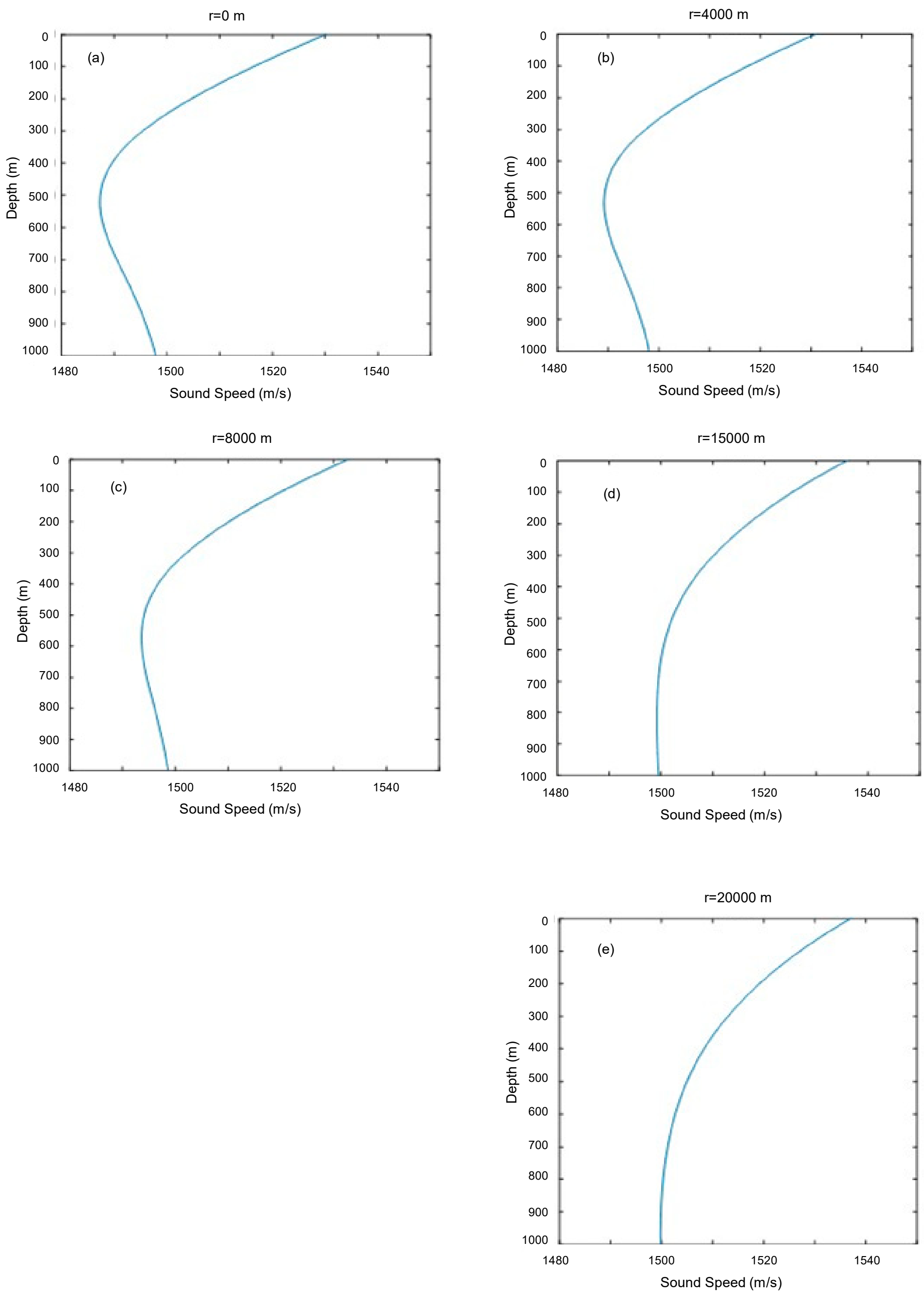

Figure 15. Variation in sound velocity gradient at different distances, (**a**) r = 0 m, (**b**) r = 4000 m, (**c**) r = 8000 m, (**d**) r = 15,000 m, (**e**) r = 20,000 m.

3.1.3. The Influence of Sound Source Frequency on Sound Propagation

In this study, we tested different frequencies to see how they affected sound propagation in seawater. Figure 16 compares the sound pressure level distribution at two frequencies, 10 Hz and 20 Hz, when DC = 20 m/s. The lower sound source frequency has no effect on the appearance of the convergence zone, but the influence of the vortex on the convergence zone becomes smaller, making it difficult to distinguish what changes have occurred. Another reason for this phenomenon is that when the frequency is reduced, the convergence effect of the sound waves appears to be smaller, and the distribution of the sound waves on the entire plane becomes more uniform, making the convergence zone less obvious.

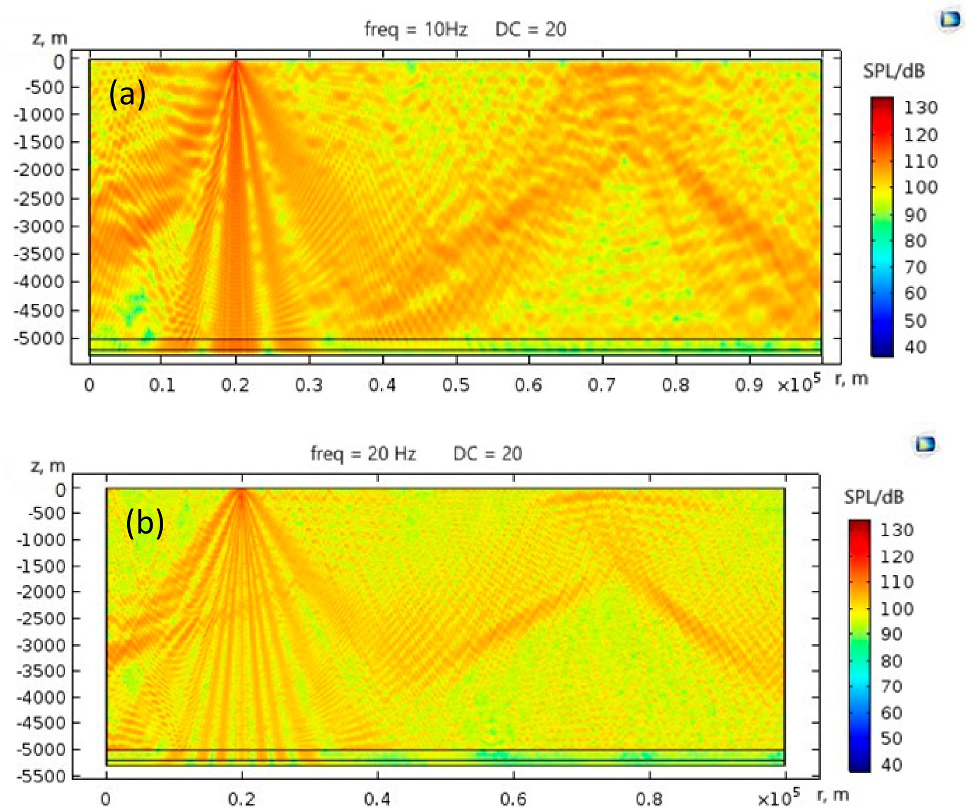

Figure 16. Sound pressure level distribution image at different frequencies when DC = 20 m/s, (**a**) f = 20 Hz, (**b**) f = 10 Hz.

Figure 17 shows related images of sound transmission loss and distance at a depth of 400 m obtained with COMSOL software at 10 Hz and 20 Hz to better explore the effect of sound source frequency on sound propagation when the vortex exists. The change trend of the sound transmission loss image tends to be the same at lower frequencies such as 10 Hz and 20 Hz, but the convergence zone effect is less obvious. Low frequencies, such as 100 Hz and 200 Hz (Figure 18a,b), have no significant effect on the convergence zone; however, as the sound source frequency rises to 1000 Hz, the convergence effect becomes more apparent than at 200 Hz (Figure 18c). The transmission loss is approximately 30 db lower than in other locations. It is possible to conclude that changing the frequency of the sound source will affect sound propagation in the vortex area, and the convergence effect of higher frequency sound waves will become stronger in this area.

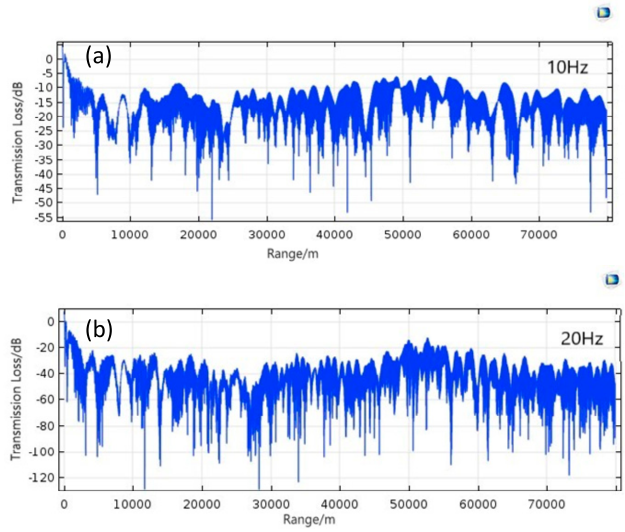

Figure 17. Sound transmission loss at different frequencies, (**a**) f = 10 Hz, (**b**) f = 20 Hz, depth 400 m (COMSOL model).

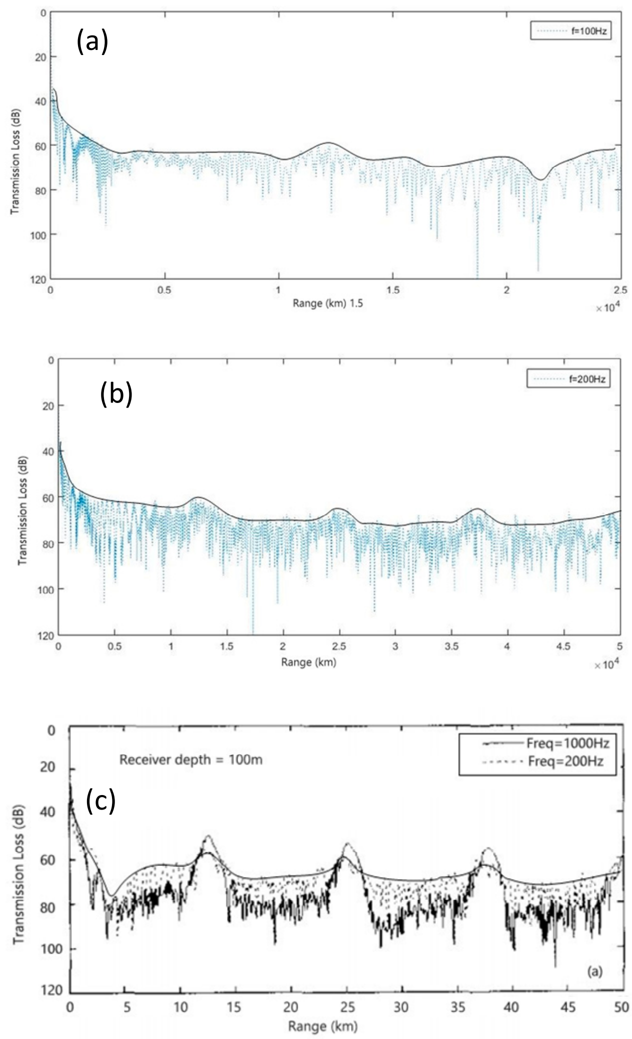

Figure 18. Sound transmission loss at different frequencies, (**a**) f = 100 Hz, 100 m depth (RAM PE Model), (**b**) f = 200 Hz, 100 m depth (RAM PE Model), (**c**) f = 200 Hz, 1000 Hz, depth 100 m (MMPE model).

4. Conclusions and Future Work

Long-term mesoscale vortices exist in the South and East China Seas, and their presence affects the sound propagation characteristics of seawater. The relevant sound propagation characteristics and sound propagation rules were studied and summarized. This has a high application value in future practical work areas such as underwater acoustic equipment research and development and tactical use. The main focus of this study was to use real time data from the AIPOcean 1.0 numerical product to identify the mesoscale vortices using the OW method, then observes the impact of mesoscale vortex on sound velocity distribution, and finally simulates the actual vortex parameters with the Gaussian vortex model in COMSOL. Finally, using this model, the impact of the presence of mesoscale vortices on the sound propagation law was investigated, yielding the following results:

(1) In a deep-sea environment where the sea surface is an absolute soft boundary and the lower seabed is a liquid seabed, the sound waves radiated by sound sources near the sea surface will reconverge at a certain distance and form a sound energy convergence zone. The cold vortex will cause the convergence zone region to move toward the sound source, reducing the width of the convergence zone; a warm vortex will cause the convergence zone region to move away from the sound source, increasing the width of the convergence zone.

(2) If the sound source is in the center of the vortex, the vortex's effect on sound propagation is more obvious, and the depth of the convergence zone is shifted downward. The reason for this is that the mesoscale vortex has the greatest impact on the sound velocity distribution at the vortex center, which has a greater impact on sound propagation. These findings also support the hypothesis that the mesoscale vortex influences sound propagation by influencing the sound velocity distribution.

The above-mentioned results are consistent with previous research using different models, confirming that our COMSOL-based model worked correctly and could be a useful tool for investigating underwater acoustic propagation in vortices. Due to the model's limitations, this study only completed the low-frequency, 2D sound field modelling and simulation. When using the COMSOL software for high-frequency or even 3D simulation, the amount of calculation increases drastically, making it difficult to process. In future research, we can try to study the effect of the vortex on the 3D sound field while solving the computational constraints in order to better fit the scale of the actual vortex.

Author Contributions: Conceptualization, Y.S., S.K. and J.H; methodology, J.H.; software, J.H.; validation, Y.S. and S.K.; formal analysis, J.H. and S.K.; investigation, S.P. and Y.S.; resources, S.P. and Y.S.; data curation, J.H. and S.K.; writing—original draft preparation, J.H. and S.K.; writing—review and editing, Y.S. and S.K.; visualization, J.H.; supervision, S.P.; project administration, S.P.; funding acquisition, YS.P. and Y.S. All authors have read and agreed to the published version of the manuscript.

Funding: This research was funded by National Key Research and Development Program of China, grant number 2016YFC1400100 and The APC was funded by Yang Song.

Acknowledgments: We acknowledge the National Key Laboratory, College of Underwater Acoustic Engineering, Harbin Engineering University, China for supporting in this research. The authors would like to thank two anonymous reviewers for their insightful and constructive comments and suggestions.

Conflicts of Interest: The authors declare no conflict of interest.

References

1. Wunsch, C.; Schmittner, A.; Chiang, J.C.H.; Hemming, S.R. The past and future ocean circulation from a contemporary perspective. *Extrem. Events* **2007**, *173*, 53–74. [CrossRef]
2. Zhang, Z.; Wang, W.; Qiu, B. Oceanic mass transport by mesoscale eddies. *Science* **2014**, *345*, 322–324. [CrossRef] [PubMed]
3. Chen, G.; Hou, Y.; Chu, X. Mesoscale eddies in the South China Sea: Mean properties, spatiotemporal variability, and impact on thermohaline structure. *J. Geophys. Res. Space Phys.* **2011**, *116*. [CrossRef]

4. Faghmous, J.H.; Frenger, I.; Yao, Y.; Warmka, R.; Lindell, A.; Kumar, V. A daily global mesoscale ocean eddy dataset from satellite altimetry. *Sci. Data* **2015**, *2*, 1–16. [CrossRef] [PubMed]
5. Li, J.; Zhang, R.; Liu, C.; Fan, H. Modeling of ocean mesoscale eddy and its application in the underwater acoustic propagation. *Mar. Sci. Bull.* **2012**, *14*, 1–15.
6. Chen, X.; Hong, M.; Zhu, W.; Mao, K.; Ge, J.J.; Bao, S. The analysis of acoustic propagation characteristic affected by mesoscale cold-core vortex based on the UMPE model. *Acoust. Aust.* **2019**, *47*, 33–49. [CrossRef]
7. Li, L.; Nowlin, W.D., Jr.; Jilan, S. Anticyclonic rings from the Kuroshio in the South China Sea. *Deep Sea Res. Part I Oceanogr. Res. Pap.* **1998**, *45*, 1469–1482. [CrossRef]
8. Wu, P.M.; Guo, X.G.; Wu, R.S. Analyses of sound velocity field in southwest sea area off Hengchun of Taiwan. *J. Oceanogr. Taiwan Strait* **2001**, *20*, 286–290. (In Chinese)
9. Available online: https://www.researchgate.net/publication/348706507_Influence_of_Mesoscale_Vortex_on_Underwater_Low-Frequency_Sound_Propagation (accessed on 22 June 2021).
10. Jian, Y.; Zhang, J.; Liu, Q.; Wang, Y. Effect of Mesoscale eddies on underwater sound propagation. *Appl. Acoust.* **2009**, *70*, 432–440. [CrossRef]
11. Okubo, A. Horizontal dispersion of floatable particles in the vicinity of velocity singularities such as convergences. *Deep Sea Res. Oceanogr. Abstr.* **1970**, *17*, 445–454. [CrossRef]
12. Weiss, J. The dynamics of enstrophy transfer in two-dimensional hydrodynamics. *Phys. D Nonlinear Phenom.* **1991**, *48*, 273–294. [CrossRef]
13. McWilliams, J.C. The emergence of isolated coherent vortices in turbulent flow. *J. Fluid Mech.* **1984**, *146*, 21–43. [CrossRef]
14. Morrow, R.; Birol, F.; Griffin, D.; Sudre, J. Divergent pathways of cyclonic and anti-cyclonic ocean eddies. *Geophys. Res. Lett.* **2004**, *31*. [CrossRef]
15. Isern-Fontanet, J.; Font, J.; García-Ladona, E.; Emelianov, M.; Millot, C.; Taupier-Letage, I. Spatial structure of anticyclonic eddies in the Algerian basin (Mediterranean Sea) analyzed using the Okubo-Weiss parameter. *Deep Sea Res. Part II Top. Stud. Oceanogr.* **2004**, *51*, 3009–3028. [CrossRef]
16. Chaigneau, A.; Gizolme, A.; Grados, C. Mesoscale eddies off Peru in altimeter records: Identification algorithms and eddy spatio-temporal patterns. *Prog. Oceanogr.* **2008**, *79*, 106–119. [CrossRef]
17. Sadarjoen, I.A.; Post, F.H. Detection, quantification, and tracking of vortices using streamline geometry. *Comput. Graph.* **2000**, *24*, 333–341. [CrossRef]
18. Doglioli, A.M.; Blanke, B.; Speich, S.; Lapeyre, G. Tracking coherent structures in a regional ocean model with wavelet analysis: Application to Cape Basin eddies. *J. Geophys. Res. Space Phys.* **2007**, *112*. [CrossRef]
19. Nencioli, F.; Dong, C.; Dickey, T.; Washburn, L.; McWilliams, J.C. A vector geometry-based eddy detection algorithm and its application to a high-resolution numerical model product and high-frequency radar surface velocities in the Southern California Bight. *J. Atmos. Ocean. Technol.* **2010**, *27*, 564–579. [CrossRef]
20. Vastano, A.C.; Owens, G.E. On the acoustic characteristics of a gulf stream cyclonic ring. *J. Phys. Oceanogr.* **1973**, *3*, 470–478. [CrossRef]
21. Weinberg, N.L.; Zabalgogeazcoa, X. Coherent ray propagation through a Gulf Stream ring. *J. Acoust. Soc. Am.* **1977**, *62*, 888–894. [CrossRef]
22. Baer, R.N. Calculations of sound propagation through an eddy. *J. Acoust. Soc. Am.* **1980**, *67*, 1180–1185. [CrossRef]
23. Chen, C.; Yang, K.-D.; Ma, Y.-L.; Duan, R. Comparison of surface duct energy leakage with bottom-bounce energy of close range propagation. *Chin. Phys. Lett.* **2016**, *33*, 104302. [CrossRef]
24. Heaney, K.D.; Campbell, R.L. Three-dimensional parabolic equation modeling of mesoscale eddy deflection. *J. Acoust. Soc. Am.* **2016**, *139*, 918–926. [CrossRef] [PubMed]
25. COMSOL Multiphysics® v.5.6. Available online: www.comsol.com (accessed on 20 August 2019).
26. Liu, Z.; Wu, X.; Xu, J.; Li, H.; Lu, S.; Sun, C.; Cao, M. China Argo project: Progress in China Argo ocean observations and data applications. *Acta Oceanol. Sin.* **2017**, *36*, 1–11. [CrossRef]
27. Yan, C.; Zhu, J.; Xie, J. An ocean data assimilation system in the Indian Ocean and west Pacific Ocean. *Adv. Atmos. Sci.* **2015**, *32*, 1460–1472. [CrossRef]
28. Cui, F.J. Mesoscale Eddies in the Sound China Sea Identification and Statistical Characteristics Analysis. Master's Thesis, Ocean University of China, Qingdao, China, 2015; pp. 20–21.
29. *Version R2017a, Copyright 1984–2015*; The MathWorks, Inc.: Natick, MA, USA, 2017; Available online: https://jp.mathworks.com/company/newsroom/mathworks-announces-release-2017a-of-the-matlab-and-simulink-pro.html (accessed on 20 August 2019).
30. MacKenzie, K.V. Nine-term equation for sound speed in the oceans. *J. Acoust. Soc. Am.* **1981**, *70*, 807–812. [CrossRef]
31. Henrick, R.F.; Siegmann, W.L.; Jacobson, M.J. General analysis of ocean eddy effects for sound transmission applications. *J. Acoust. Soc. Am.* **1977**, *62*, 860–870. [CrossRef]
32. Munk, W.H. Sound channel in an exponentially stratified ocean, with application to SOFAR. *J. Acoust. Soc. Am.* **1974**, *55*, 220. [CrossRef]